

MIDAS: A MODULAR SOFTWARE FOR INTAKE FLOW DISTORTION ANALYSIS

Tommaso Piovesan[1], Alexandros Giannouloudis[1], Josep Hueso Rebassa[1], Matteo Migliorini[1], Pavlos Zachos[1] & David MacManus[1]

[1]Faculty of Engineering & Applied Sciences, Centre for Aeronautics, Propulsion & Power, Cranfield University, UK

Abstract

Modern aircraft intakes are required to operate under highly distorted flow conditions arising from compact installations, crosswind operation, ground vortices, boundary-layer ingestion, and complex intake geometries. The analysis of intake distortion often relies on heterogeneous datasets and fragmented post-processing workflows, requiring various different software tools to perform data analysis. To address these challenges, the Modular Intake Distortion Analysis Software (MIDAS) was developed at Cranfield University as a Python-based framework for the unified analysis of intake flow distortion data. MIDAS provides automated routines for the calculation of conventional and Society of Automotive Engineers (SAE) total-pressure and swirl distortion descriptors, frequency-domain analysis, engine-order harmonic analysis, and a range of visualization and data-export capabilities. The framework supports Computational Fluid Dynamics (CFD) datasets, Stereo Particle Image Velocimetry (S-PIV) measurements, and pressure-rake data through a flexible and extensible architecture. In this work, the capabilities of MIDAS are demonstrated using representative CFD, S-PIV, and pressure-rake datasets, while validation is performed against analytical test cases and published SAE methodologies. The results demonstrate that MIDAS provides a consistent and reproducible workflow for intake distortion assessment, significantly reducing post-processing effort while enabling direct comparison between experimental and computational datasets within a single software environment.

Keywords: Intake flow distortion, data analysis, Python

1. Introduction

Modern aircraft propulsion systems would be exposed to complex and highly non-uniform inlet flow conditions which arise from a variety of sources, including intake geometry [1] , crosswind operation [2]-[6], aircraft manoeuvres at high angles of attack [7]-[10], boundary-layer ingestion [11], ground-vortex ingestion [12]-[15], and flow separation within compact intake configurations [16]-[18]. These distortions result in non-uniform distributions of total pressure, velocity, and swirl angle at the Aerodynamic Interface Plane (AIP) between the intake and the engine [19], potentially reducing performance and operability range while increasing aerodynamic and structural loading on downstream compressor and fan stages [20]-[25].

Historically, intake distortion assessment has focused primarily on total-pressure distortion through the use of conventional descriptors such as Intake Pressure Recovery (IPR), Distortion Coefficient (DC60), Inlet Distortion Circumferential Coefficient (IDC), and Inlet Distortion Radial Coefficient (IDR) [19][26]. More recently, the importance of swirl distortion has received increasing attention due to its influence on compressor stability, rotating stall inception, and overall engine operability [27]-[29]. This is supported by advances in experimental techniques such as Stereoscopic Particle Image Velocimetry (S-PIV), which can capture high-resolution, time-resolved velocity fields [30][31]. In contrast to conventional rake measurements, S-PIV provides full-field velocity information with significantly higher spatial and temporal resolution, allowing the calculation of swirl angle directly from velocity components across the entire measurement plane [32]. In parallel, advances in high-fidelity Computational Fluid Dynamics (CFD) simulations have highlighted the importance of unsteady distortion phenomena, which cannot be fully characterized using time-averaged metrics

alone [33]. Frequency-domain analyses, harmonic descriptors, and engine-order assessments have therefore become increasingly important for understanding the interaction between distorted inlet flows and turbomachinery blade response.

Despite these developments, intake distortion investigations often rely on fragmented post-processing workflows involving multiple software packages, custom scripts, and manual data manipulation. Moreover, experimental and computational datasets are frequently processed using different methodologies, making direct comparison difficult and increasing the risk of inconsistencies. Furthermore, modern CFD and Particle Image Velocimetry (PIV) campaigns can generate very large datasets, creating additional challenges for data management, processing productivity and data archiving.

To address these challenges, a bespoke Modular Intake Distortion Analysis Software (MIDAS) was developed (**Figure 1**). MIDAS is a unified Python framework for intake flow distortion analysis and provides a modular and extensible software environment capable of processing CFD, PIV, and pressure-rake datasets using a common workflow. The software allows data import, distortion descriptor evaluation, frequency-domain analysis, engine-order harmonic analysis, visualization, and data export within a single platform. Particular emphasis has been placed on flexibility, allowing users to extend existing functionalities and adapt the framework to new dataset formats or distortion analysis methodologies. This paper presents the architecture, implementation, validation, and demonstration of MIDAS. The software capabilities are first described, followed by verification against analytical benchmark cases and previous SAE methodologies. Finally, representative CFD, PIV, and pressure-rake datasets are used to demonstrate the applicability of the framework to a range of intake distortion investigations.

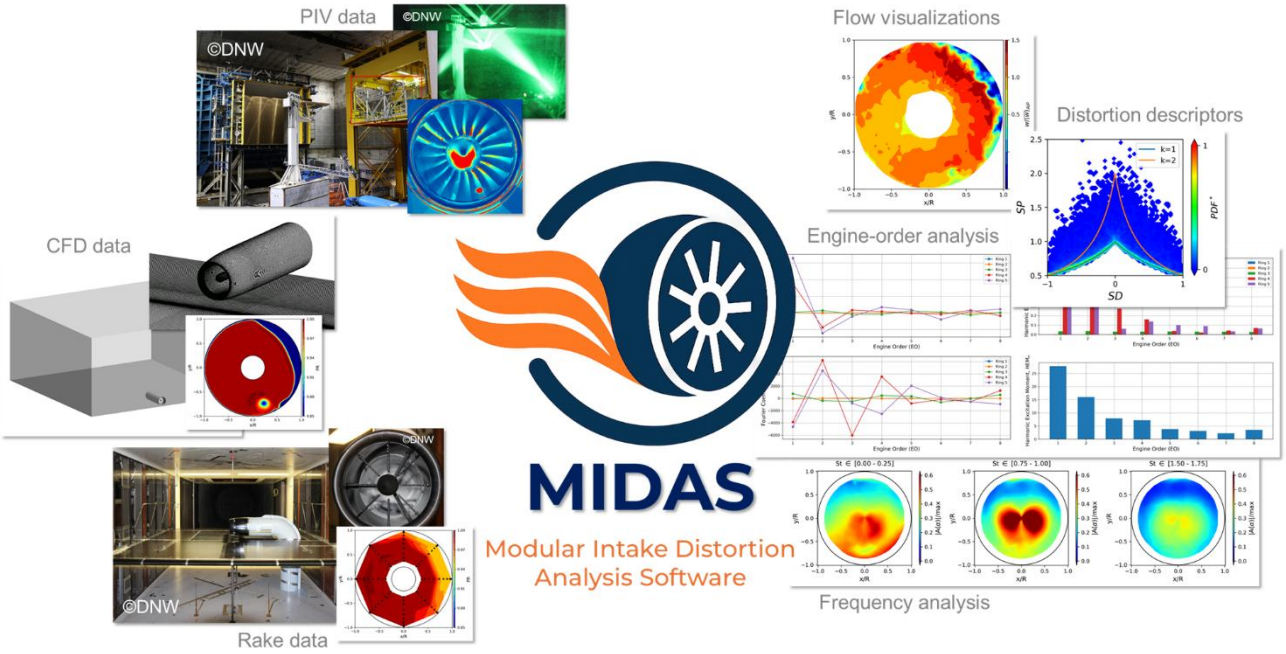


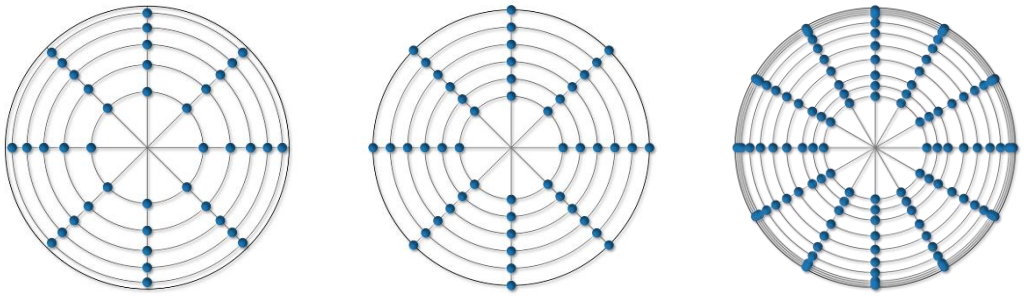
Figure 1 – MIDAS general overview of capabilities.

2. Analysis Methodology and Distortion Metrics

2.1 Aerodynamic Interface Plane Discretization and Area Averaging

Fan face flow distortion characterization relies on discretization of the fan face plane (or Aerodynamic Interface Plane, AIP) into a discrete number of radial rings and circumferential rakes. The calculation of area-averaged quantities and subsequently inlet flow distortion descriptors is typically conducted using these locations [34] [35]. The AIP can be discretized using equal-area rings, equally spaced radial locations, or user-defined radial and circumferential distributions to match experimental rake

geometries (Figure 2). These discretization variations are all implemented within the MIDAS software and processing of both CFD and experimental datasets while maintaining consistency with established industrial distortion-assessment methodologies.



(a) (b) (c)

Figure 2 – Ring-rake configurations available in MIDAS for the evaluation of area-averaged quantities and distortion descriptors. The sampling locations can be arranged using (a) an equal-area distribution, (b) an equi-spaced distribution, or (c) a user-defined custom distribution.

To calculate the area-averaged quantities at the AIP, the flow variables are first interpolated onto the selected ring-rake grid. Let ϕ denote a generic flow variable; the circumferentially averaged value at radial position i is obtained as:

$$\phi_i = \frac{1}{n_\theta} \sum_{j=1}^{n_\theta} \phi_{i,j} \tag{1}$$

where n_θ is the number of circumferential locations and ϕ is the value of the variable at radial position r_i and circumferential location θ_j. Area-averaged quantities at the AIP are subsequently calculated using an area-weighted averaging procedure:

$$\bar{\phi} = \frac{\sum_{i=1}^{n_r} \phi_i A_i}{\sum_{i=1}^{n_r} A_i} \tag{2}$$

where A_i is the area associated with ring i and n_r is the number of radial positions.

2.2 Inlet Distortion Descriptors

To assess inlet flow distortion, MIDAS computes a suite of established and user-defined distortion metrics. These descriptors quantify the spatial non-uniformity of total pressure, swirl angle, and other relevant flow variables, and provide metrics for characterizing area-averaged, sectoral, and both circumferential and radial distortion.

To calculate the distortion descriptors based on a given flow variable, area-weighted averages are first evaluated within circumferential sectors of angular extent θ, applied at each radial ring about the discretization points. For sector-based metrics, such as the Distortion Coefficient DCθ, this procedure yields sector-averaged values at each radial location within the sector. These ring-wise sector values are subsequently combined, and the sector is then rotated circumferentially around the annulus. Depending on the formulation, the minimum and/or maximum values over all sector positions are then extracted to define the final distortion metric.

2.2.1 Total Pressure Distortion Descriptors

For the assessment of total-pressure distortion at the Aerodynamic Interface Plane, MIDAS implements both conventional [19] and SAE-standard [34] descriptors. The conventional descriptors implemented in MIDAS include:

- Intake Pressure Recovery (IPR),

- Distortion Coefficient (DCθ),
- Distortion Index (DI),
- Inlet Distortion Circumferential Coefficient (IDC),
- Inlet Distortion Radial Coefficient (IDR).

The Intake Pressure Recovery (IPR) quantifies the overall total-pressure loss through the intake and is defined as the ratio between the area-averaged total pressure at the AIP and the freestream total pressure:

$$IPR = \frac{p_{0,AIP}}{P_{0,\infty}} \tag{3}$$

The Distortion Coefficient (DCθ) quantifies the severity of the most distorted circumferential sector of angular extent θ, normalized by the area-averaged dynamic pressure at the AIP:

$$DC60 = \frac{\overline{p_{0,AIP}} - \overline{p_{0,\theta}}}{\overline{q_{AIP}}} \tag{4}$$

In most applications, a sector width of 60° is used, resulting in the widely known DC60. The Distortion Index (DI) provides a global measure of total-pressure non-uniformity and is calculated from the difference between the maximum and minimum total pressures across the AIP, normalized by the face-average total pressure. To distinguish between circumferential and radial distortion components, the Inlet Distortion Circumferential Coefficient (IDC) and the Inlet Distortion Radial Coefficient (IDR) are calculated. The IDC descriptor quantifies circumferential pressure non-uniformity on a ring-by-ring basis, whereas IDR characterizes radial variations in total pressure between the inner and outer regions of the AIP.

In addition to the conventional descriptors, MIDAS implements the methodology defined in SAE AIR1419 [34] for the assessment of inlet total pressure distortion. The SAE AIR1419 methodology evaluates distortion independently for each ring of the rake configuration and characterizes both the intensity and topology of the distortion pattern. The implemented descriptor elements include:

- Circumferential Distortion Intensity $(\Delta PC/P)_i$,
- Circumferential Distortion Extent $(\theta\text{-})_i$,
- Multiple-Per-Revolution $(MPR)_i$,
- Radial Distortion Intensity $(\Delta PR/P)_i$.

The Circumferential Distortion Intensity $(\Delta PC/P)_i$ quantifies the magnitude of the low-pressure region relative to the ring-average total pressure. The Circumferential Distortion Extent $(\theta\text{-})_i$ defines the angular extent of the low-pressure sector. The Multiple-Per-Revolution descriptor $(MPR)_i$ identifies the effective number of low-pressure regions around the circumference, while the Radial Distortion Intensity $(\Delta PR/P)_i$ quantifies the deviation of the ring-average pressure from the overall face-average pressure. Together, these descriptors provide a detailed description of both circumferential and radial pressure distortion.

2.2.2 Swirl Distortion Metrics

To quantify AIP swirl distortion the swirl distortion descriptors proposed by the SAE S-16 committee [35] are used. Although total-pressure distortion assessment is well established, swirl distortion characterization remains an active area of research due to the limited availability of high-resolution experimental measurements. Nevertheless, these descriptors have been successfully applied to the analysis of intake flow distortion [36]-[38]. The calculation of the descriptors is based on the swirl angle, defined as the deviation of the local flow direction from the axial direction:

$$\alpha = \tan^{-1}\left(\frac{v_\theta}{w}\right) \tag{5}$$

where v_θ is the circumferential velocity component and w is the axial velocity component. The swirl angle distribution is evaluated along the concentric rings at the AIP. For each ring, three SAE swirl descriptors are calculated within MIDAS:

- Swirl Intensity (SI), which quantifies the overall magnitude of the swirl distortion.
- Swirl Directivity (SD), which indicates the dominant swirl direction.
- Swirl Pairs (SP), which characterizes the circumferential structure of the distortion by identifying the effective number of alternating positive and negative swirl regions.

The descriptors are calculated by identifying positive and negative swirl sectors around each ring. For each sector, average positive and negative sector swirl values (SS+ and SS-) are determined from the circumferential swirl-angle distribution. These quantities are subsequently combined according to the SAE methodology to calculate the ring-based swirl descriptors:

$$SI_i = \frac{SS_i^+\theta_i^+ + |SS_i^-|\theta_i^-}{360} \tag{6}$$

$$SD_i = \frac{SS_i^+\theta_i^+ + SS_i^-\theta_i^-}{SS_i^+\theta_i^+ + \left|SS_i^-\right|\theta_i^-} \tag{7}$$

$$SP_i = \frac{SS_i^+\theta_i^+ + |SS_i^-|\theta_i^-}{2\max(SS_i^+\theta_i^+, \left|SS_i^-\right|\theta_i^-)} \tag{8}$$

The methodology is applicable to both simple distortion patterns containing a single swirl pair and more complex patterns containing multiple positive-negative swirl pairs distributed around the circumference. Representative swirl descriptors for the entire AIP are obtained through area-weighted averaging of the ring-based values:

$$SI = \frac{\sum_{i=1}^{n_r} SI_i A_i}{\sum_{i=1}^{n_r} A_i} \tag{9}$$

$$SD = \frac{\sum_{i=1}^{n_r} SD_i A_i}{\sum_{i=1}^{n_r} A_i} \tag{10}$$

$$SP = \frac{\sum_{i=1}^{n_r} SP_i A_i}{\sum_{i=1}^{n_r} A_i} \tag{11}$$

where A_i is the area associated with ring i and nr is the total number of rings. For time-resolved datasets, the descriptors may be evaluated for each instantaneous snapshot and subsequently averaged to obtain mean swirl-distortion characteristics.

2.3 Frequency and Engine-Order Analysis

Along with the implementation of distortion descriptors, MIDAS includes frequency-domain analysis capabilities for the investigation of unsteady intake flows. These tools are applicable to both experimental and computational time-resolved datasets and allow the identification of dominant frequencies, periodic flow structures, and engine-order excitation mechanisms that may contribute to compressor or fan aerodynamic forcing.

For time-resolved datasets, MIDAS can perform Fast Fourier Transform (FFT) analysis using standard scientific Python libraries. The analysis can be applied to any scalar or vector quantity available in the dataset, including velocity components, total pressure, static pressure, and swirl

angle. The resulting frequency spectra enables the identification of dominant frequencies associated with flow instabilities. In addition to FFT analysis, MIDAS can calculate Power Spectra (PS) and Power Spectral Density (PSD) distributions using established spectral estimation techniques available in the Python scientific ecosystem. Spectral analyses can be performed using user-defined windowing functions, segment lengths, and overlap settings to improve the resolution.

MIDAS also supports engine-order (EO) analysis for the assessment of inlet distortion effects on turbomachinery forced-response excitation. Flow non-uniformities entering compressors or fans generate circumferential variations in total pressure and swirl that can excite blade vibration modes at specific engine orders. Quantifying these harmonic components is therefore important when assessing potential aerodynamic forcing mechanisms and aero-mechanical interactions. The engine-order analysis implemented in MIDAS follows the methodology described by the SAE ARP6912 document [39]. Circumferential distributions of total pressure or swirl angle at the AIP are decomposed into Fourier harmonics. For each ring, the Fourier coefficients a_n and b_n are calculated and used to determine the resultant forcing magnitude:

$$V_{n,i} = \sqrt{a_{n,i}^2 + b_{n,i}^2} \tag{12}$$

where *n* is the harmonic order (or Engine Order, EO) and i denotes the radial ring position. The forcing magnitude in terms of total pressure can then be normalized to obtain the Harmonic Excitation Index (HEI), which provides a non-dimensional measure of the excitation strength associated with a given engine order. In its most common form, the HEI is normalized by the Aerodynamic Interface Plane-averaged dynamic pressure:

$$HEI_{n,i} = \frac{V_{n,i}}{\overline{q_{AIP}}} \tag{13}$$

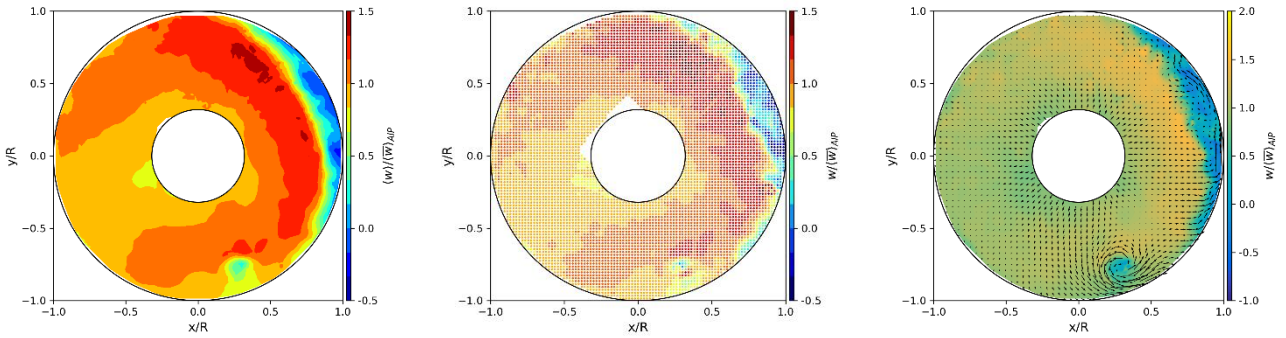
Higher HEI values indicate stronger circumferential distortion patterns and therefore greater potential aerodynamic forcing on rotating blades. When considering swirl distortion, the Harmonic Swirl Index (HSI) can be determined (see [39]), which is equivalent to the forcing magnitude calculated from swirl-angle circumferential variations.

To quantify the overall excitation level across the Aerodynamic Interface Plane, MIDAS also calculates the Harmonic Excitation Moment (HEM) and Harmonic Swirl Moment (HSM), which combines the harmonic excitation levels from all radial locations using an appropriate radial weighting as defined in [39]. The HEM and HSM provide a single descriptor representative of the global forcing potential associated with a given engine order. The engine-order analysis capabilities available in MIDAS complement conventional intake distortion descriptors by providing information on the harmonic content of the flow field and its potential impact on turbomachinery forced-response behaviour.

2.4 Flowfield Data Visualization Methods

MIDAS includes a comprehensive set of visualization tools designed to support the analysis and interpretation of intake flow distortion datasets. These tools enable the visualization of both steady and unsteady flow fields and allow the export of processed data for further analysis using external software packages.

One of the primary visualization capabilities of MIDAS is the generation of contour and scatter plots of flow variables. The software can produce visualizations of time-averaged flow fields, standard deviation distributions, and instantaneous flow snapshots. Plot layouts are fully customizable, allowing users to define contour levels, color maps, annotations, rake overlays, and velocity-vector overlays according to specific analysis requirements. Examples of contour visualizations generated by MIDAS are shown in Figure 3.



(a) (b) (c)

Figure 3 – Contour plots generated by MIDAS, based on data published in [36], showing: (a) the time-averaged flow field (filled contours using Delaunay triangulation), (b) an instantaneous flow field (scatter plot), and (c) an instantaneous flow field displayed with an alternative colormap and color scale, with superimposed velocity vectors.

For time-variant datasets, MIDAS can automatically generate temporal animations from sequences of static PNG images of instantaneous flows. Individual snapshots exported as image files are combined into video formats such as AVI or MP4. These animations provide a convenient means of visualizing the temporal evolution of flow structures, vortex motion, and distortion patterns, particularly for highly unsteady intake flows.

To better characterize complex distortion patterns and quantify flow unsteadiness, MIDAS includes a routine for the generation of the so-called joint Probability Density Function (j-PDF) maps [37][38]. These maps illustrate the relationship between two distortion descriptors by representing the relative frequency at which specific combinations of values occur at the AIP (Figure 4).

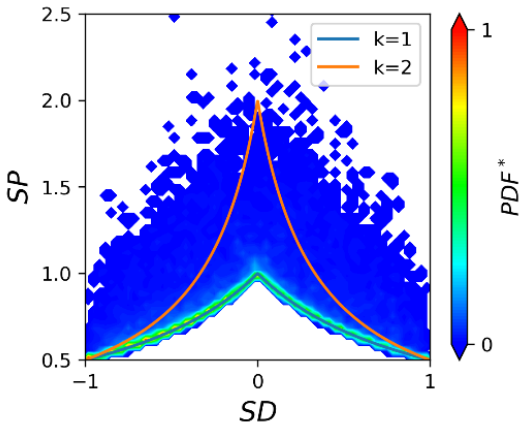


Figure 4 – Example of a joint probability density function (j-PDF) map generated in MIDAS for SAE SP and SD distortion descriptors using unsteady velocity fields at the exit of an S-duct [40].

The j-PDF approach provides considerably more information than simple time-averaged quantities by revealing the range and variability of the flow distortion. For a pair of descriptors X and Y, the descriptor ranges are discretized into equally spaced intervals, with the resolution selected according to the descriptor being considered. The probability of observing a particular distortion pattern is obtained by integrating the probability density function over the selected descriptor ranges:

$$P[X_A \leq X \leq X_B, Y_A \leq Y \leq Y_B] = \int_{Y_A}^{Y_B} \int_{X_A}^{X_B} PDF(X,Y) dX, dY \tag{14}$$

where X_A, X_B, Y_A, and Y_B denote the lower and upper limits of the descriptor ranges. To facilitate comparisons between different datasets and operating conditions, the probability density function is

non-dimensionalized as:

$$PDF^* = \frac{PDF}{[max(X) - min(X)][max(Y) - min(Y)]} \tag{15}$$

Frequency-domain analysis can be extended through the generation of Strouhal-band visualizations (Figure 5), which provide a means of relating dominant frequency content to characteristic flow length scales and velocities and are particularly useful for comparing flow phenomena across different operating conditions and intake geometries. In this approach, frequency-domain results obtained from FFT or power spectral density (PSD) analysis are converted into Strouhal number using a representative length scale L and reference velocity V, as follows:

$$St = \frac{fL}{V} \tag{16}$$

where f is the frequency.

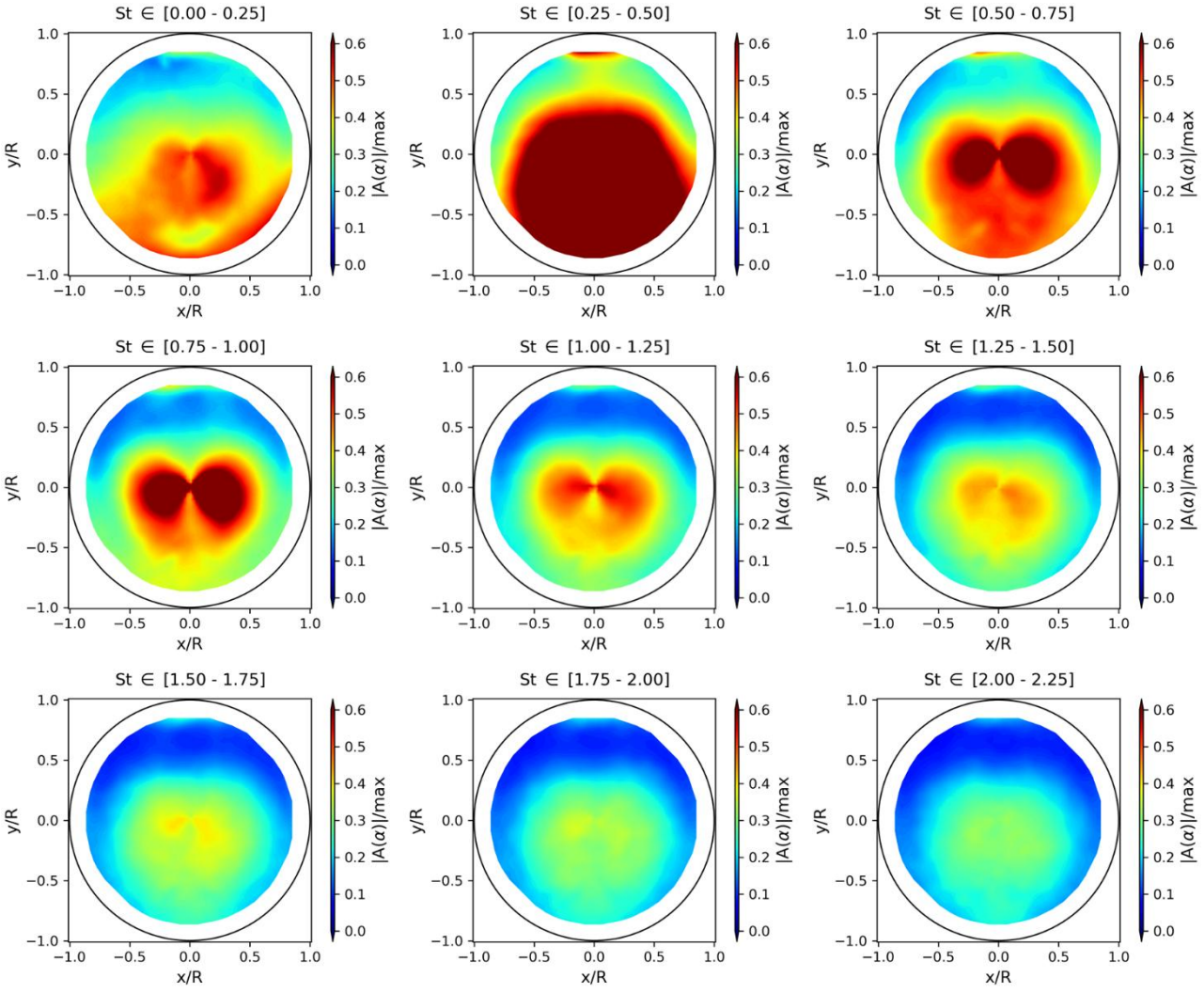


Figure 5 – Example of Strouhal number bands obtained from FFT analysis of the swirl angle distribution with data reported in [40].

Finally, MIDAS includes several data-export utilities to facilitate interoperability with external postprocessing tools. Processed datasets and derived flow variables can be exported in Tecplot-compatible formats [41], allowing users to perform additional visualization using commercial or in-house software packages. This capability provides flexibility while maintaining a consistent data-processing workflow within the MIDAS framework.

3. Software Architecture

3.1 Development Philosophy

The Modular Intake Distortion Analysis Software (MIDAS) was developed to provide a flexible, user-friendly, and extensible framework for the analysis of flow distortion using both computational and experimental datasets. The software was written in Python and developed using the Anaconda scientific computing environment, while being distributed with standard Python dependencies to simplify installation and distribution across other industrial and research institutions.

The development philosophy of MIDAS is based on four principles: *modularity*, *extensibility*, *reproducibility*, and *workflow automation*. Modularity was the primary design cornerstone during the development of MIDAS. The software was developed using a modular architecture in which individual functionalities are separated into independent Python *modules* (*.py* files). This approach simplifies the software structure and facilitates debugging and future development, while allowing users to selectively activate only the required analysis and post-processing routines. The modular structure also enables developers to integrate custom analysis scripts or plotting routines without modifying the core framework. Each module performs a dedicated task, such as data import, distortion descriptor calculation, statistical processing, or visualization. This organization improves code readability, facilitates collaborative development, and allows individual components of the software to be updated independently.

Extensibility was considered essential to ensure that MIDAS could evolve alongside future research and industrial requirements. The software architecture was designed to support the integration of additional analysis methods and processing capabilities with minimal modification to the existing core codebase. New distortion descriptors, analysis methods, or visualization tools can therefore be incorporated efficiently without restructuring the overall framework.

Reproducibility was also treated as a key requirement throughout the software development process. MIDAS relies on predefined input files to ensure that analyses can be reproduced consistently across different datasets. Moreover, to improve traceability and reproducibility, the user input files are automatically copied and timestamped during execution, allowing the same analysis configuration to be reused at a later stage for the same or different datasets.

Workflow automation was another central principle of the MIDAS development philosophy. The software was developed to automate repetitive analysis tasks and reduce manual intervention during large-scale data processing activities. User-defined input files determine which cases are analyzed, which calculations are executed, and which plots are generated, allowing large batches of datasets to be processed automatically with minimal user interaction. During execution, the software automatically loads the input datasets, identifies file formats, executes selected analysis routines, calculates flow variables and distortion descriptors, generates plots or exports processed data, and stores all results in a structured Hierarchical Data Format (HDF5 or *.h5*) file. This workflow-oriented approach significantly reduces processing time, improves analysis consistency, and minimizes the risk of user-induced errors during data handling and post-processing operations.

3.2 Software Structure

MIDAS is organized as a structured collection of folders designed to separate user input files, data files, Python modules, and generated outputs. The overall structure of the software is shown in Figure 6.

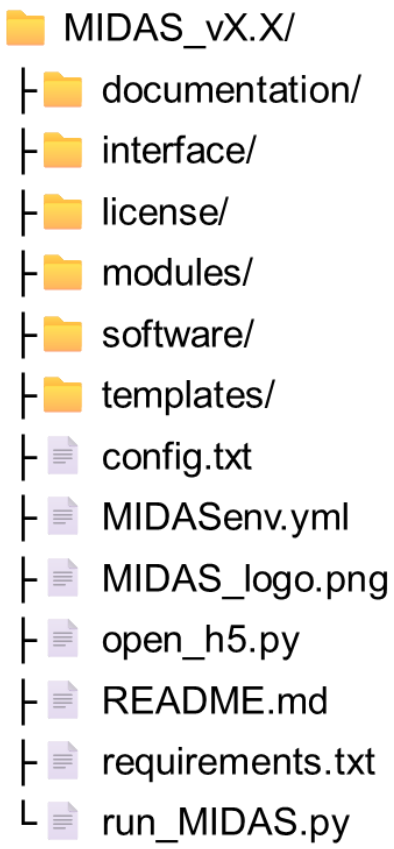


Figure 6 – Overview of the MIDAS folder structure.

The **documentation** folder contains the user manual and all supporting technical documentation required for installation and configuration of the software. The **interface** folder provides examples of user input files, illustrating the available functionalities and serving as templates for user-defined cases. The **license** folder contains all files related to software licensing. The **modules** directory contains the core Python source code (.py files), which implements data reading, data processing, analysis routines, and visualization functionalities. The **software** folder contains installation resources, including Python and Anaconda installation files. The **templates** directory provides standardized input file templates that ensure consistent data formatting across different projects. These templates are intended to help users correctly structure CFD or experimental datasets prior to analysis, ensuring compatibility with the MIDAS processing framework. The configuration file (*config.txt*) defines global execution settings, including:

- the path to the MIDAS modules directory,
- the main result file name (.h5 file),
- the input data folder location,
- activation of the post-processing routine,
- activation of the plotting routine.

The *MIDASenv.yml* file defines the Conda-based software environment used during development and can also be used by users running MIDAS with Anaconda and Spyder to ensure consistency of package versions across different releases and projects. The *requirements.txt* file defines the Python package dependencies required for standard installation without Anaconda. The *run_MIDAS.py* script serves as the main entry point for executing the software, while the *open_h5.py* script provides utilities for reading the HDF5 output files.

3.3 Execution Workflow

The execution workflow of MIDAS, illustrated in Figure 7, is controlled through a set of user-defined input files that define the analysis process in a structured manner.

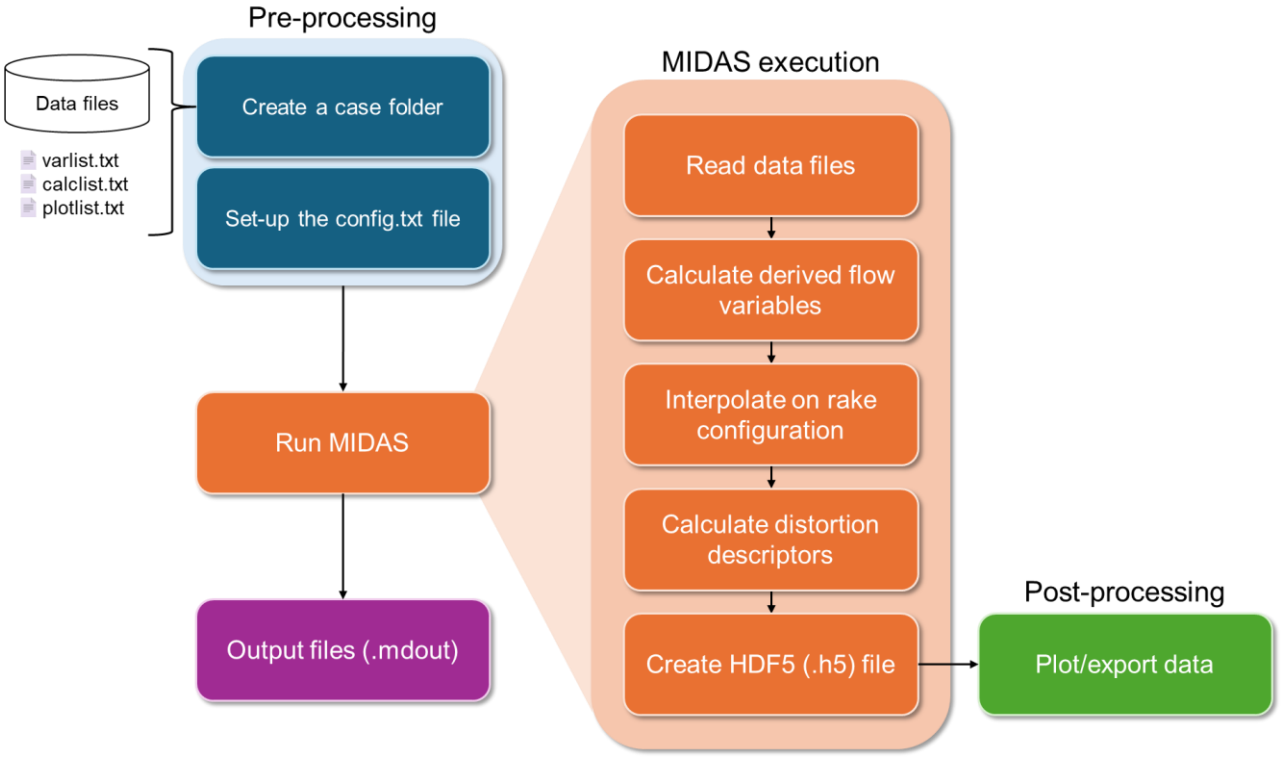


Figure 7 – Schematic illustrating MIDAS execution workflow.

To execute a MIDAS case, the user must perform the following steps:

- Create a case folder within the main MIDAS directory.
- Set up the required input files (*varlist.txt*, *calclist.txt*, and *plotlist.txt*).
- Configure the main configuration file (*config.txt*) by specifying the path to the modules directory and the data folder location.
- Launch the execution by running *run_MIDAS.py* via the command window, Anaconda Prompt, or a Python IDE (e.g., Spyder).

The structure of each case folder is standardized and must follow the format shown in Figure 8.

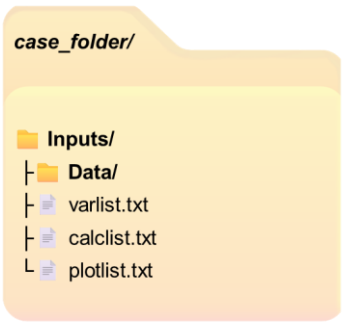


Figure 8 – Standardized structure of MIDAS case folder.

The input files define the variables to be imported, the calculations to be performed, and the post-processing operations to be executed. The variable list file (*varlist.txt*) defines how input datasets should be interpreted. With it, the user can specify the mapping between input file columns and variable names, define the dataset structure, and specify whether the data is steady or unsteady, as well as whether it originates from experimental measurements or numerical simulations.

The calculation list file (*calclist.txt*) defines the analysis workflow by specifying which computational functions are called during processing. Functions within the modules are invoked using keyword-based calls. Available operations include:

- masking of PIV data based on user-defined filtering criteria,
- computation of derived flow variables from the input dataset,
- evaluation of vorticity components normal to the measurement plane,
- detection of vortical structures using Q-criterion or λ_2 methods,
- calculation of turbulence quantities such as turbulent kinetic energy (TKE) and Reynolds stresses,
- temporal averaging of instantaneous data fields,
- generation of rake grids and data interpolation for the calculation of area-averaged variables and descriptors,
- computation of area-averaged flow quantities,
- evaluation of conventional intake distortion descriptors [19],
- calculation of SAE total pressure distortion descriptors [34],
- calculation of SAE swirl distortion descriptors [35],
- calculation of SAE harmonic distortion descriptors [39].

The plot list file (*plotlist.txt*) defines the visualization routines to be executed. At present, supported outputs include:

- contour and scatter plots of selected variables,
- joint probability density function (PDF) maps for pairs of descriptors,
- frequency analysis and Strouhal band visualizations,
- export of datasets to Tecplot-compatible formats,
- generation of videos from PNG image sequences (useful for transient datasets),
- visualization of Fourier coefficients and harmonic indices.

All results are automatically saved in an **Outputs** directory created during execution. An example of output directory is shown in Figure 9. The output directory contains a timestamped run folder that stores all results generated during execution. This includes the main HDF5 results file (*h5file_.h5*), a human-readable summary of its contents (*h5file_info.txt*), and timestamped copies of the user input files (*calclist_XXXX* and *varlist_XXXX*) to ensure reproducibility of the analysis. In addition, a set of .mdout files is generated, containing, for example, the computed distortion descriptors. These files are generated and structured in such a way to facilitate further post-processing of results.

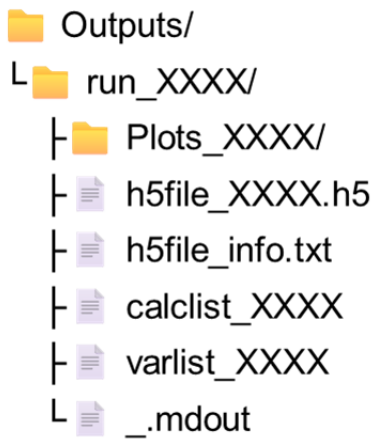


Figure 9 – Example of the MIDAS output folder structure.

3.4 Supported Input Data, Formats, and Output Files

MIDAS supports multiple experimental and computational data formats, enabling, for example, the analysis of datasets generated by different CFD solvers. The flexible input handling routines also allow users to implement additional functions for reading new data formats, making the framework suitable for a wide range of projects. The software currently supports:

- Computational Fluid Dynamics (CFD) datasets,
- Particle Image Velocimetry (PIV) measurements,
- pressure rake and probe measurements,
- steady-state datasets,
- time-variant datasets,
- three-dimensional flow-field data extracted on circular planes.

MIDAS includes flexible data import routines capable of handling multiple file structures and formatting conventions. Supported features include:

- automatic delimiter recognition,
- automatic header detection,
- flexible column mapping,
- support for structured and tabulated datasets.

The software supports common ASCII-based file formats, including .txt, .dat, and .csv. The flexible data handling capabilities allow MIDAS to interface with a wide range of CFD solvers and post-processing tools commonly used in intake flow distortion studies. Currently supported input formats are summarized in Table 1. Both input and processed data are stored in Hierarchical Data Format (HDF5). HDF5 files (*.h5*) provide efficient and portable storage for large datasets while preserving a structured hierarchy similar to folders and subfolders, as shown in Figure 10. The generated HDF5 result files are automatically saved in the Outputs directory, timestamped to uniquely identify each execution, and structured according to the analyses performed. To minimize memory usage and improve processing efficiency when handling large datasets, MIDAS only requires a reduced set of input variables. The minimum input quantities are the velocity components (u, v, w), the static temperature T, and the static pressure p. From these quantities, MIDAS can compute a range of derived flow variables (Figure 11), including for example swirl angle, α, Mach number Ma, total temperature T0, total pressure p0, dynamic pressure q, and density ρ.

Table 1 – Supported input data formats currently compatible with MIDAS.

Format	Description
BLOCK	Data written variable-by-variable
POINT	Data written point-by-point
ANSYS Fluent	Fluent export format (.dat)
Tecplot BLOCK	Tecplot block-formatted data
Tecplot POINT	Tecplot point-formatted data
IJ-ordered	Grid-based ordering using I and J indices (for PIV data)
I-ordered	Sequential point ordering using index I
Rake data (ASCII)	Rake measurement data

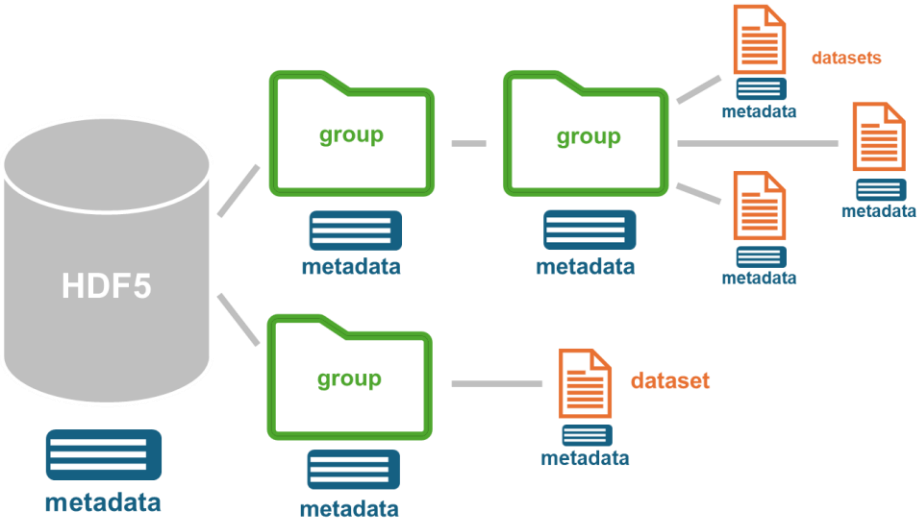


Figure 10 – Example structure of a MIDAS HDF5 results file showing the hierarchical organization of processed datasets.

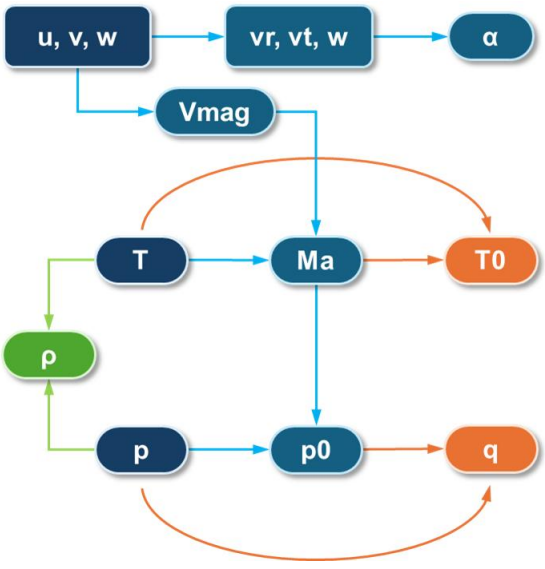


Figure 11 – Examples of derived flow variables computed in MIDAS from the minimum required inputs (velocity components, static temperature, and static pressure).

3.5 Development, Distribution, and Licensing

As previously described, the software was developed using Anaconda due to its advantages for scientific computing applications, including access to precompiled scientific libraries, simplified installation of complex dependencies such as NumPy, SciPy, and PyTables, stable and tested package configurations, reduced dependency conflicts, simplified environment management using Conda, and optimized performance for numerical workloads. For software distribution, MIDAS is deployed using standard Python dependencies defined in the requirements.txt file. This approach removes the dependency on Anaconda for end users and provides a smaller installation footprint, reduced IT and cybersecurity restrictions in corporate environments, transparent dependency management, and simplified installation in restricted environments. To improve performance and protect intellectual property, Python modules are compiled using Cython into .pyd files. Compared with standard Python source files (.py) and Python bytecode files (.pyc), .pyd files provide improved source-code protection, faster execution performance, and simplified software distribution. A time-limited licensing system is also implemented to control authorized usage of the software. During execution, MIDAS validates the software license against a predefined expiry date and restricts operation outside approved usage periods, ensuring controlled distribution.

4. Verification

MIDAS script verification was performed using a series of manufactured analytical test cases and reference cases available in the literature. The objective of the validation process was to verify the correct implementation of the conventional intake distortion descriptors, SAE total-pressure descriptors, SAE swirl descriptors, and SAE harmonic descriptors within the software framework. For each validation category, analytical or reference solutions were compared against the results generated by MIDAS. Only representative cases are presented in this section for brevity, although multiple validation cases were investigated during software development. The validation cases were selected to cover different distortion topologies, rake configurations, and descriptor calculation methodologies.

4.1 Conventional Total Pressure Distortion Descriptors

One of the test cases used to verify the implementation of conventional total-pressure distortion descriptors consisted of a manufactured total-pressure distortion pattern representative of a ground-vortex-type intake distortion on a 12 x 12 rake configuration. The distortion field was constructed using prescribed total-pressure losses superimposed onto a reference pressure field. The reference total pressure was set to $p_{0,ref}$ = 101,340 Pa, with a dynamic pressure q = 20,000 Pa and a static pressure p = 78,736 Pa. The distortion descriptors were evaluated using a circumferential resolution of 30°. A visualization of the manufactured distortion pattern is shown in Figure 12.

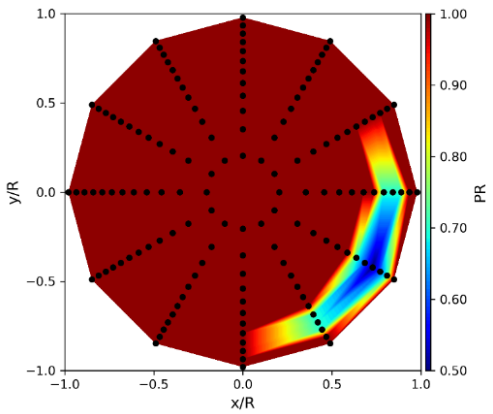


Figure 12 – Prescribed total-pressure distortion pattern used for the validation of conventional distortion descriptors calculation.

The analytical reference values and the corresponding MIDAS results are summarized in Table 2. The comparison demonstrates the capability of MIDAS to accurately calculate conventional intake distortion descriptors commonly used in intake distortion assessments.

Table 2 – Validation results for the calculation of conventional total-pressure distortion descriptors.

Descriptor	Analytical	MIDAS
DC60	0.461	0.461
DI	0.513	0.513
IDC	0.372	0.372
IDR	-0.026	-0.026
IPR	0.974	0.974

4.2 SAE Swirl Distortion Descriptors

The SAE swirl distortion descriptor implementation was validated using a series of manufactured swirl patterns reported in SAE AIR5686, "*A Methodology for Assessing Inlet Swirl Distortion*" [35]. For brevity, only one representative validation case is presented in this section. The selected case corresponds to a twin two-per-revolution swirl distortion pattern generated on a rake configuration composed of 9 rings and 72 circumferential rakes. The imposed swirl field consisted of two identical swirl pairs periodically distributed over 360°, with a swirl amplitude of 8.66° per swirl lobe. A schematic representation of the imposed swirl distortion pattern is shown in Figure 13. The resulting SAE swirl descriptors calculated analytically and using MIDAS are compared in Table 3.

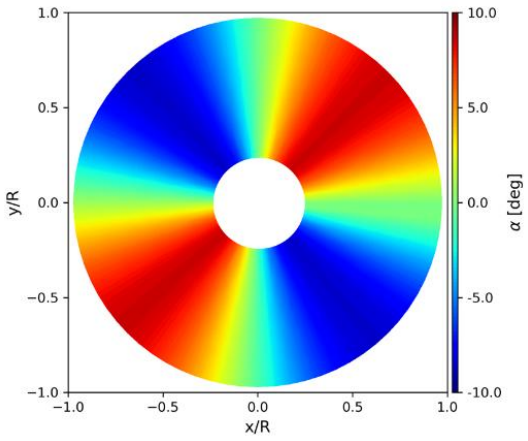


Figure 13 – Twin two-per-revolution swirl distortion pattern used for the validation of SAE swirl descriptor calculation [35].

Table 3 – Validation results for the calculation of SAE swirl distortion descriptors.

Descriptor	Result in [35]	MIDAS
SI	5.77°	5.42°
SD	0.0	0.0
SP	2	2

The agreement between analytical and computed values confirms the correct implementation of the SAE swirl descriptor methodology within MIDAS. The observed difference in swirl intensity arises from the way the descriptor is evaluated. In [35], it is reported at a single radial position, whereas in MIDAS it is computed using both swirl angle and the area associated with each probe. As a result, the area weighting of each measurement point influences the final value.

4.3 SAE Total Pressure Distortion Descriptors

The implementation of the SAE total-pressure distortion descriptors was validated using reference test cases taken from SAE AIR1419, *"Inlet Total-Pressure Distortion Considerations for Gas-Turbine Engines"* [34]. Multiple reference cases were evaluated during development, although only one representative aircraft-type distortion pattern is presented here.

The validation case used an equal-area rake configuration composed of 8 circumferential rakes and 5 radial rings. The distortion pattern reproduced the aircraft-type total-pressure distribution provided in SAE AIR1419. The corresponding total-pressure distortion field is shown in Figure 14. The analytical reference values and MIDAS results for the ring-based SAE descriptors are summarized in Table 4 and Table 5, respectively. The results demonstrate that MIDAS correctly calculates the SAE AIR1419 total-pressure distortion metrics across all radial positions.

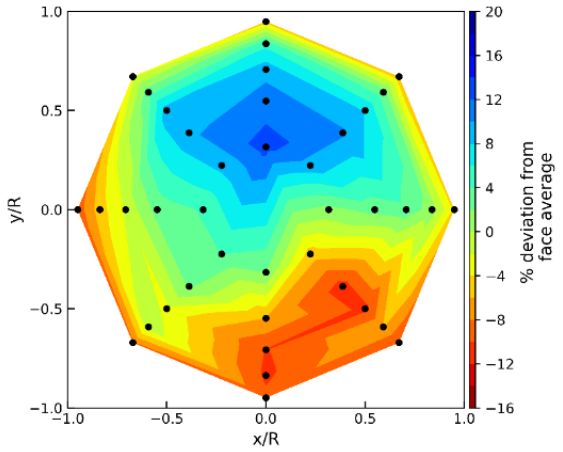


Figure 14 – Aircraft-type total-pressure distortion pattern used for the validation of SAE total pressure descriptor calculation [34].

Table 4 – Reference values used for the validation of SAE total-pressure distortion descriptor calculation [34].

Ring	ΔPC/P	θ- (deg)	MPR	ΔPR/P
1	0.0327	203.2	1.0000	-0.0463
2	0.0574	174.6	1.0000	-0.0275
3	0.0624	180.5	1.0000	-0.0056
4	0.0394	180.2	1.0000	0.0117
5	0.0236	177.8	1.0000	0.0678

Table 5 – MIDAS results for SAE total-pressure distortion descriptors.

Ring	ΔPC/P	θ- (deg)	MPR	ΔPR/P
1	0.0327	203.2	1.0000	-0.0463
2	0.0574	174.6	1.0000	-0.0275
3	0.0624	180.5	1.0000	-0.0056
4	0.0394	180.2	1.0000	0.0117
5	0.0236	177.8	1.0000	0.0678

4.4 SAE Harmonic Descriptors

The implementation of the SAE harmonic descriptors was validated using manufactured harmonic distortion test cases developed according to SAE ARP6912 *"Substantiation of Power Available and Inlet Distortion Compliance for Rotorcraft Engine Inlet Barrier Filter Installations"* [39]. Four validation cases were investigated using different total-pressure and swirl distributions and rake configurations. Only one representative case is presented here.

The selected validation case employed a rake configuration composed of 8 circumferential rakes and 5 radial rings. The objective of the test case was to validate the calculation of harmonic coefficients, resultant forcing magnitudes, Harmonic Excitation Indices (HEI), and Harmonic Excitation Moments (HEM). The analytical resultant forcing magnitude V_n and the corresponding MIDAS results are summarized in Table 6 and Table 7, respectively. The harmonic coefficients a_n and b_n, and the Harmonic Excitation Indices (HEI) and Harmonic Excitation Moments (HEM) were also evaluated for all radial locations and are shown in Figure 15. The close agreement between analytical solutions and MIDAS results confirms the correct implementation of the SAE AIR8458 harmonic descriptors and demonstrates the capability of MIDAS to evaluate harmonic distortion characteristics relevant to turbomachinery forced-response assessments.

Table 6 – Analytical values of the resultant forcing magnitude V(n,i). Data from [39].

$V_{n,i}$	n=1	n=2	n=3	n=4
r_1	0.03937	0.07701	0.01768	0.05750
r_2	0.04635	0.10198	0.00518	0.04500
r_3	0.09992	0.11800	0.01915	0.02500
r_4	0.05396	0.06865	0.04199	0.02000
r_5	0.09464	0.06042	0.01715	0.04000

Table 7 – Verified MIDAS results for the resultant forcing magnitude V(n,i) using the data from [39].

$V_{n,i}$	n=1	n=2	n=3	n=4
r_1	0.03937	0.07702	0.01768	0.05750
r_2	0.04635	0.10198	0.00518	0.04500
r_3	0.09992	0.11800	0.01915	0.02500
r_4	0.05396	0.06865	0.04199	0.02000
r_5	0.09464	0.06042	0.01715	0.04000

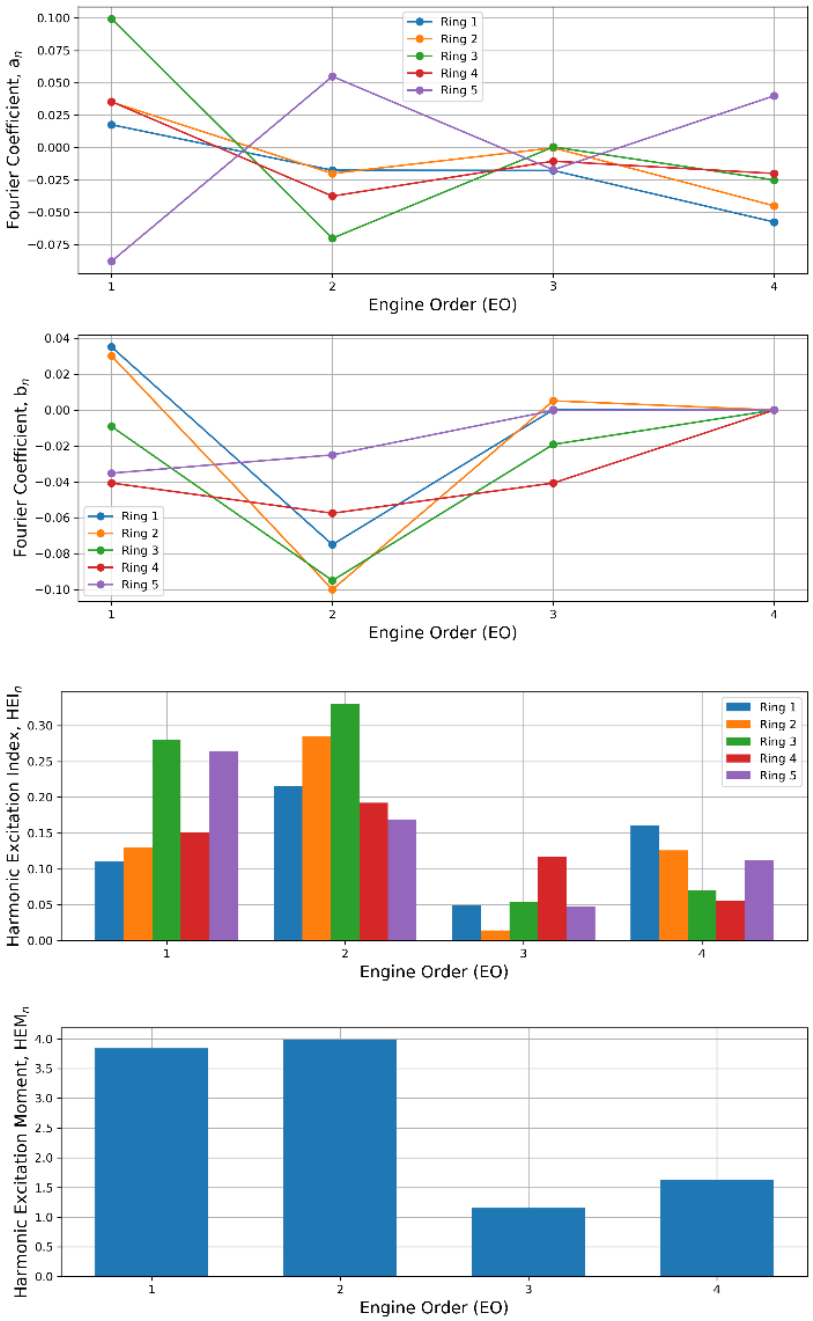


Figure 15 – Plots of the Fourier coefficients a_n and b_n (top) and bar plots of the HEI and HEM (bottom) used to validate the implementation of the harmonic descriptors in MIDAS.

5. Demonstration Cases

To demonstrate the capabilities and flexibility of MIDAS, three representative intake distortion datasets are presented in this section. These include a Computational Fluid Dynamics (CFD) dataset, an experimental Stereo Particle Image Velocimetry (S-PIV) dataset, and experimental rake probe measurements. The selected cases illustrate the ability of MIDAS to process both numerical and experimental data originating from different acquisition techniques and data structures while applying a unified post-processing and distortion analysis framework.

For all cases, the datasets were processed using the latest version of MIDAS to ensure consistency in post-processing methodology, descriptor calculation, plotting style, and data visualization. The demonstration cases highlight the capability of MIDAS to compute conventional and SAE-defined distortion descriptors, generate visualization outputs, and process both steady and time-resolved datasets.

5.1 S-PIV Dataset

The first demonstration case consists of an experimental Stereo Particle Image Velocimetry (S-PIV) dataset obtained for a powered intake operating under crosswind conditions above a ground plane. The measurement plane was located inside the intake approximately 30 mm upstream of the fan face. The dataset consists of 1,000 phase-locked snapshots acquired using a low-bandwidth S-PIV system, with approximately 7,000 three-dimensional velocity vectors available per snapshot. The original dataset and preliminary results were previously presented in [36].

The measured variables include the spatial coordinates (x, y) and the three velocity components (u, v, w), from which additional quantities such as velocity magnitude, swirl angle, turbulence quantities, and distortion descriptors were computed using MIDAS. The dataset was processed using a ring-rake configuration composed of five equal-area rings and eight circumferential rakes, following SAE recommendations [35]

The results presented in this section include time-averaged distributions of axial velocity and swirl angle at the Aerodynamic Interface Plane (AIP), as shown in Figure 16. Instantaneous distributions of normalized axial velocity and swirl angle are also presented in Figure 17 to illustrate the unsteady nature of the intake flow distortion. In addition, MIDAS was used to generate joint probability density function (j-PDF) maps of the swirl descriptors, as shown in Figure 18.

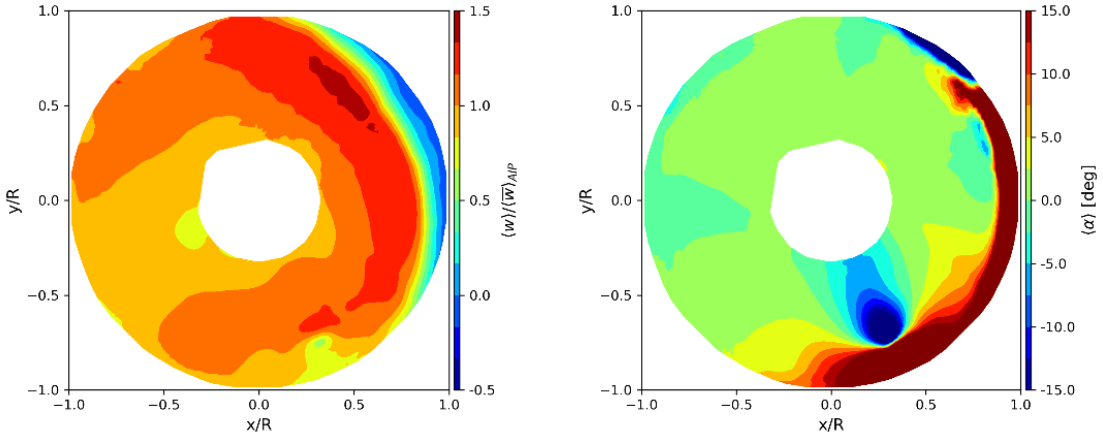


Figure 16 – Time-averaged distributions of axial velocity (left) and swirl angle (right) at the Aerodynamic Interface Plane (AIP) [36].

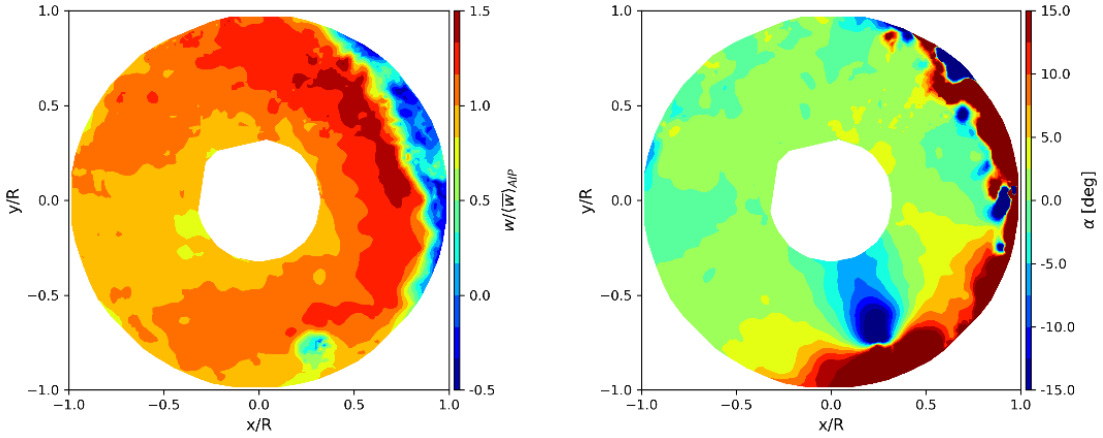


Figure 17 – Instantaneous distributions of axial velocity (left) and swirl angle (right) at the Aerodynamic Interface Plane (AIP) [36].

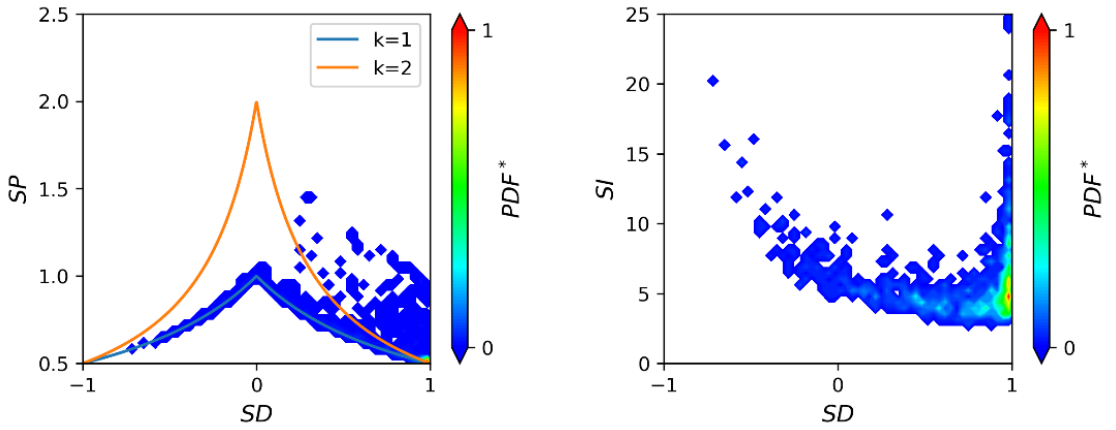


Figure 18 – Joint probability density function (j-PDF) maps for SP–SD (left) and SD–SI (right) for the fourth ring [36].

5.2 CFD Dataset

The second demonstration case consists of a steady-state CFD simulation of an aspirated intake operating under crosswind conditions above a ground plane. The simulation was performed using ANSYS Fluent [41] with the Reynolds-Averaged Navier-Stokes (RANS) approach and the k-ω SST turbulence model [42]. The analysis plane corresponds to a cross-sectional plane located inside the intake at the Aerodynamic Interface Plane (AIP). The original CFD results were previously presented in [43].

The exported CFD dataset includes the spatial coordinates (x, y, z), velocity components (u, v, w), static pressure p, total pressure p0, static temperature T, and total temperature T0. MIDAS was used to compute conventional total pressure distortion descriptors and SAE swirl distortion descriptors. The distortion descriptors were evaluated using a ring-rake configuration composed of five equal-area rings and 72 circumferential rakes. The resulting distributions of axial velocity, swirl angle, and normalized total pressure ratio at the AIP are presented in Figure 19. In addition, SAE harmonic descriptors were calculated, including the harmonic excitation index (HEI) and harmonic excitation moment (HEM), as illustrated in Figure 20.

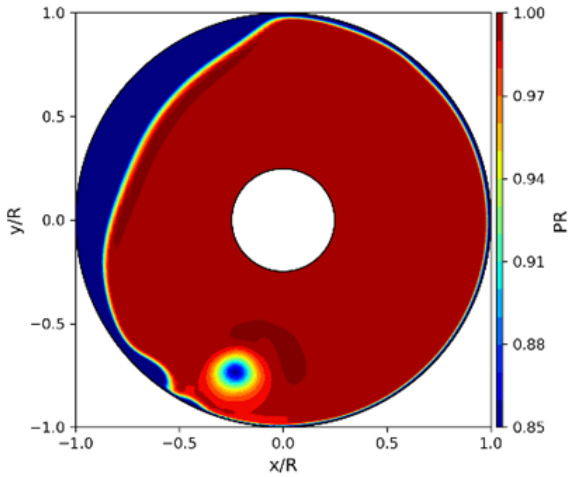


Figure 19 – Resulting distributions of total pressure recovery coefficient for an intake at crosswind conditions [43].

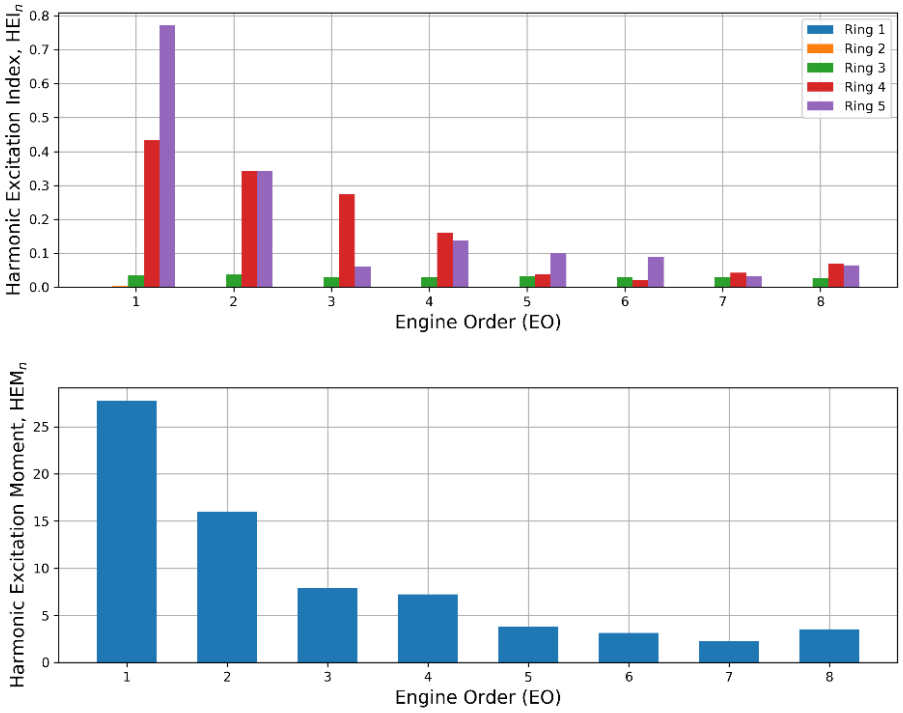


Figure 20 – Resulting HEI and HEM bar plots for rings 1 to 5 and the first eight engine orders.

5.3 Rake Probe Data

The third demonstration case consists of experimental rake total pressure probe measurements acquired for an aspirated intake operating under crosswind conditions above a ground plane. The measurements were performed on a cross-sectional plane located inside the intake using a rake arrangement composed of 80 probes distributed across 10 rings with 8 circumferential positions per ring. The original experimental data and preliminary analyses were previously presented in [43].

The measured dataset contains the probe spatial locations (x, y) together with steady-state total pressure values. MIDAS was used to process the probe data, plot the total pressure distribution, and compute total-pressure distortion descriptors. The descriptor calculations were performed using a grid of 24 rakes and 10 rings. The resulting normalized total-pressure ratio distribution at the AIP is shown in Figure 21, while the corresponding conventional distortion metrics, including DC60 and Intake Pressure Recovery (IPR), are summarized in Table 8.

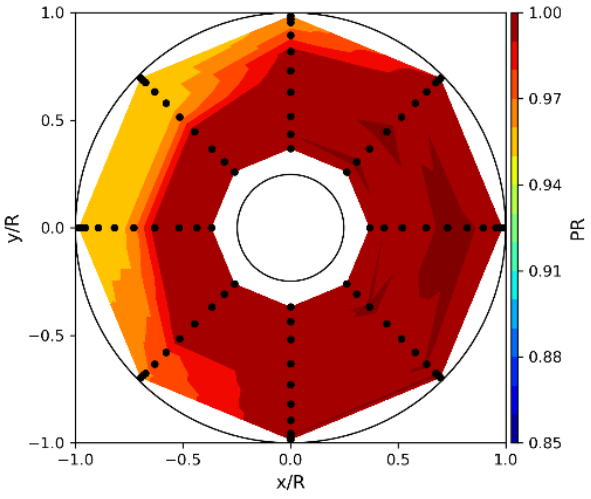


Figure 21 – Resulting distribution of total pressure ratio plotted at rake resolution.

Table 8 – Calculated conventional total pressure distortion descriptors.

Descriptor	Value
DC60	0.649
DI	0.049
IDC	0.032
IDR	0.013
IPR	0.990

6. Conclusions

The Modular Intake Distortion Analysis Software (MIDAS) has been developed as a unified and extensible framework for the analysis of intake flow distortion from experimental and computational datasets. The software integrates data import, distortion descriptor evaluation, frequency-domain analysis, engine-order harmonic analysis, visualization, and data-export capabilities within a single workflow, thereby reducing the reliance on multiple post-processing tools and custom analysis scripts. MIDAS supports a broad range of data sources, including CFD simulations, Stereo Particle Image Velocimetry (S-PIV) measurements, and pressure-rake datasets. Conventional and SAE-standard descriptors are implemented for the evaluation of total-pressure distortion, swirl distortion, and aeromechanical distortion descriptors, allowing direct comparison between datasets from different analysis techniques. Built-in visualization and export features facilitate the interpretation and communication of results while maintaining a reproducible and robust processing workflow. The capabilities of MIDAS have been demonstrated using representative CFD, PIV, and pressure-rake datasets, verified against analytical benchmark cases and published SAE test cases. MIDAS accurately reproduces established distortion metrics while providing a consistent framework for the analysis of steady and unsteady, as well as numerical and experimental, datasets. The modular architecture of MIDAS has been intentionally designed to support future development and expansion. Ongoing and planned extensions include modules for extreme-value analysis of distortion events, pressure-field reconstruction from velocity measurements, automated ground-vortex characterization, and Proper Orthogonal Decomposition (POD). These developments will further extend the applicability of the framework to a broader range of engine-integration and intake-distortion assessment requirements. By combining multiple distortion-analysis methodologies within a single platform, MIDAS provides a practical tool for researchers and engineers working in intake aerodynamics, engine performance, stability, and operability. The framework enables more efficient processing of large datasets, improves analysis consistency and reproducibility, and facilitates direct comparison between experimental and computational investigations, thereby supporting the design, development, and testing of distortion-tolerant propulsion systems.

7. Acknowledgements

Initial versions of MIDAS were developed under the project NIFTI which received funding from the CLEAN SKY 2 Joint Undertaking (JU) under Grant Agreement no. 864911. The JU receives support from the European Union's Horizon 2020 research and innovation programme and the CLEAN SKY 2 JU members other than the Union.

8. Contact Author Email Address

tommaso.piovesan@cranfield.ac.uk

9. Copyright Statement

The authors confirm that they, and their company or organization, hold copyright on all of the original material included in this paper. The authors also confirm that they have obtained permission, from the copyright holder of any third-party material included in this paper, to publish it as part of their paper. The authors confirm that they give permission or have obtained permission from the copyright holder of this paper, for the publication and distribution of this paper as part of the ICAS proceedings or as individual off prints from the proceedings.

References

[1] Wellborn S R, Reichert B A and Okiishi T H. Study of the compressible flow in a diffusing S-duct. Journal of Propulsion and Power, Vol. 10, No. 5, pp. 668–675, 1994.

[2] Quémard C, Garçon F and Raynal J-C. High Reynolds number air intake tests in the ONERA F1 and S1MA wind tunnels. Proc Workshop on Airframe Engine Integration at DLR, 1996.

[3] Colin Y, Aupoix B, Boussuge J F and Chanez P. Numerical simulation and analysis of crosswind inlet flows at low Mach numbers. Proc 8th International Symposium on Experimental and Computational Aerothermodynamics of Internal Flows, 2007.

[4] Zhang M. Numerical investigation of nacelle intake flow distortion at crosswind conditions. Proc 32nd Congress of the International Council of the Aeronautical Sciences (ICAS 2021), Shanghai, China, 2021.

[5] Lecordix J L, Mullender A, Lecossais E, Godard J L and Hepperle M. Hybrid laminar flow nacelle design. Technical Report, 1996.

[6] Harjes L, Bode C, Grubert J, Frantzheld P, Koch P and Friedrichs J. Investigation of jet engine intake distortions caused by crosswind conditions. Journal of the Global Power and Propulsion Society, Vol. 4, pp. 48–62, 2020.

[7] Larkin M J and Schweiger P S. Ultra high bypass nacelle aerodynamics inlet flow-through high angle of attack distortion test. NASA-CR-189149, NASA, 1992.

[8] Hodder B, Farquhar B and Dudley M. A large-scale investigation of engine influence on inlet performance at angle-of-attack. Proc 1st Flight Test Conference, Las Vegas, Nevada, USA, 1981.

[9] Mohankumar B, Hall C A and Wilson M J. Sweep effects on fan–intake aerodynamics at high angle of attack. Journal of Turbomachinery, Vol. 144, No. 10, 2022.

[10] Mohankumar B, Hall C A and Wilson M J. Fan aerodynamics with a short intake at high angle of attack. Journal of Turbomachinery, Vol. 143, No. 5, pp. 1–10, 2021.

[11] Kawai R, Friedman D and Serrano L. Blended Wing Body Boundary Layer Ingestion Inlet Configuration and System Studies. NASA CR-2006-214534, NASA, 2006.

[12] Johns C. The aircraft engine inlet vortex problem. Proc AIAA Aircraft Technology, Integration and Operations (ATIO) Technical Forum, Los Angeles, California, USA, 2002.

[13] Murphy J P and MacManus D G. Ground vortex aerodynamics under crosswind conditions. Experiments in Fluids, Vol. 50, No. 1, pp. 109–124, 2011.

[14] Wang Z and Gursul I. Unsteady characteristics of inlet vortices. Experiments in Fluids, Vol. 53, No. 4, pp. 1015–1032, 2012.

[15] Courtine S, Bouchet J-P, Guibert A, Gauducheau B, Mendonca E Costa R and Raynal S. Experimental characterization of intake ground vortex ingestion under crosswind conditions in wind tunnel. Proc 56th 3AF International Conference on Applied Aerodynamics, Toulouse, France, 2022.

[16] Peters A, Spakovszky Z S, Lord W K and Rose B. Ultrashort nacelles for low fan pressure ratio propulsors. Journal of Turbomachinery, Vol. 137, No. 2, 2015.

[17] Gunn E J, Brandvik T and Wilson M J. Fan-intake coupling with conventional and short intakes. Proc ASME Turbo Expo 2021: Turbomachinery Technical Conference and Exposition, Virtual, Online, 2021.

[18] Boscagli L, Christie R, MacManus D and Piovesan T. Aerodynamics of a short intake in crosswind. Aerospace Science and Technology, Vol. 129, 2022.

[19] Bissinger N C and Breuer T. Basic principles – Gas turbine compatibility – Intake aerodynamic aspects. In: Encyclopedia of Aerospace Engineering. Wiley, pp. 1–10, 2010.

[20] di Mare L, Simpson G and Sayma A I. Fan forced response due to ground vortex ingestion. Proc ASME Turbo Expo 2006: Power for Land, Sea and Air, Barcelona, Spain, 2006.

[21] Green J S. Forced response of a large civil fan assembly. Proc ASME Turbo Expo 2008: Power for Land, Sea and Air, Berlin, Germany, 2008.

[22] Williams D D. Review of current knowledge on engine response to distorted inflow conditions. AGARD-CP-400, AGARD, 1986.

[23] Wartzek F, Brandstetter C, Holzinger F and Schiffer H-P. Response of a transonic compressor to a massive inlet distortion. Proc 11th European Conference on Turbomachinery Fluid Dynamics and Thermodynamics, Madrid, Spain, 2015.

[24] Chennuru V Y T, Corral R, Rodríguez-Blanco S, Vahdati M and Zhao F. Fan non-synchronous forced vibration under crosswind. Journal of Turbomachinery, Vol. 147, No. 5, 2025.

[25] Chennuru V Y T, Corral García R, Zhao F, Rodríguez-Blanco S and Vahdati M. Impact of fan aerodynamics on inlet distortion at crosswind. Proc ASME Turbo Expo 2025: Turbomachinery Technical Conference and Exposition, Memphis, Tennessee, USA, 2025.

[26] Pecinka J, Bugajski G, Kmoch P and Jílek A. Jet engine inlet distortion screen and descriptor evaluation. Acta Polytechnica, Vol. 57, pp. 22–31, 2017.

[27] Aulehla F. Intake swirl – A major disturbance parameter in engine/intake compatibility. Proc 13th Congress

of the International Council of the Aeronautical Sciences, Seattle, Washington, USA, 1982.

[28]Pazur W and Fottner L. The influence of inlet swirl distortions on the performance of a jet propulsion two-stage axial compressor. Journal of Turbomachinery, Vol. 113, No. 2, pp. 233–240, 1991.

[29]Meyer W, Pazur W and Fottner L. The influence of intake swirl distortion on the steady-state performance of a low bypass, twin-spool engine. AGARD-CP-498, AGARD, 1991.

[30]Doll U, Migliorini M, Kapulla R, MacManus D G and Lawson N J. Non-intrusive flow diagnostics for unsteady inlet flow distortion measurements in novel aircraft architectures. Progress in Aerospace Sciences, Vol. 130, 2022.

[31]Kompenhans J et al. Particle image velocimetry in aerodynamics: Technology and applications in wind tunnels. Journal of Visualization, Vol. 2, pp. 229–244, 2000.

[32]Kempaiah K U et al. High-resolution turbofan intake flow characterization by automated stereoscopic-PIV in an industrial wind tunnel environment. Measurement Science and Technology, Vol. 35, No. 2, 2023.

[33]Burnazzi M, Probst A and Steger M. Hybrid RANS/LES of an isolated engine nacelle with crosswind using an unstructured CFD solver. Proc Progress in Hybrid RANS-LES Modelling, Vol. 143, pp. 347–356, 2020.

[34]SAE S-16 Committee. Inlet total-pressure distortion considerations for gas-turbine engines. SAE AIR1419D, Revision D, Society of Automotive Engineers, 2023.

[35]SAE S-16 Committee. A methodology for assessing inlet swirl distortion. SAE AIR5686, Society of Automotive Engineers, 2022.

[36]Piovesan T, Zachos P K and MacManus D. Unsteady swirl distortion characterization in a coupled fan-intake system in crosswind conditions using stereoscopic particle image velocimetry. Proc AIAA SciTech Forum, 2026.

[37]Gil-Prieto D, MacManus D G, Zachos P K and Bautista A. Assessment methods for unsteady flow distortion in aero-engine intakes. Aerospace Science and Technology, Vol. 72, pp. 292–304, 2018.

[38]Migliorini M, Zachos P K, MacManus D G and Haladuda P. S-duct flow distortion with non-uniform inlet conditions. Proceedings of the Institution of Mechanical Engineers, Part G: Journal of Aerospace Engineering, Vol. 237, No. 2, pp. 357–373, 2023.

[39]SAE International. Substantiation of Power Available and Inlet Distortion Compliance for Rotorcraft Engine Inlet Barrier Filter Installations. SAE ARP6912, Society of Automotive Engineers, 2023.

[40]Migliorini M. Impact of Inlet Conditions on Unsteady Flow Distortion for Complex Aero-Engine Intakes. PhD Thesis, Cranfield University, United Kingdom, 2021.

[41]Tecplot Inc. Tecplot 360 Data Format Guide, Release 2025 R2, 2025.

[42]Menter F. Zonal two equation k-ω turbulence models for aerodynamic flows. Proc 23rd Fluid Dynamics, Plasmadynamics and Lasers Conference, Orlando, Florida, USA, 1993.

[43]Piovesan T, Zachos P and MacManus D. Total Pressure Distortion Reconstruction Methods from Velocimetry Data within an Aero-engine Intake at Crosswind. Proc 16th European Conference on Turbomachinery Fluid Dynamics and Thermodynamics (ETC2025), 2025.